International Journal of High-Rise Buildings
June 2020, Vol 9, No 2, 155-166
https://doi.org/10.21022/IJHRB.2020.9.2.155

International Journal of
High-Rise Buildings
www.ctbuh-korea.org/ijhrb/index.php

# Experimental Test on the Effect of Onsite Welding of Steel Plates for a Joint Between Concrete Columns and a Steel Belt Truss

**Hak Bo Shim[1], Da Yo Yun[2], and Hyo Seon Park[2]**

[1]*Research & Development Institute, Lotte Engineering & Construction, Seoul 137-903, Korea*
[2]*Department of Architectural Engineering, Yonsei University, Seoul 120-749, Korea*

**Abstract**

To connect exterior reinforced concrete (RC) columns with the steel belt truss, the gusset plates are welded to the steel plates embedded in the RC column. Then, the concrete around an embedded plate is very likely to be damaged by the heat input from a long-time (6 to 48 hours) welding of the embedded and gusset plates at a joint between RC columns and steel belt truss. However, very few studies have assessed the concrete damage caused by the welding heat between embedded and gusset plates, and no clear onsite solution has been found. In this paper, experimental tests have been carried out on 4 full-scale specimen to analyze the effect of long-time (about 6 hours) onsite welding (1-side welding and 3-side welding) between a gusset plate and an embedded plate in high strength concrete with compressive strength of 55 MPa and 80 MPa on RC columns. The effect of the long-time welding heat of embedded and gusset plates, which are used in real high-rise building construction sites, on concrete is analyzed in terms of the following three items: 1) temperature distribution, 2) pattern and characteristics of cracks, and 3) effect of the cracks on the compressive strength of RC column. Based on the experimental results, even though the heat input up to about 150? from the long-time onsite welding on the high-strength concrete column for the joint could result in concrete cracks in a radial form, it is found that the welding cracks have no effect on the axial stiffness and strength of the concrete column.

**Keywords:** Embedded plate, construction method, construction detail, high-rise building

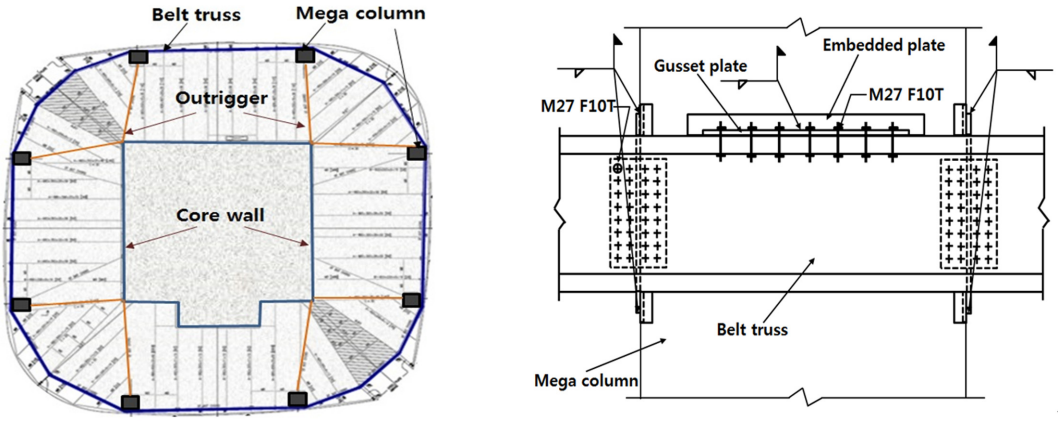
## 1. Introduction

To connect exterior RC columns with the steel belt truss in a high-rise building, the gusset plates are welded to the steel plates embedded in the RC mega column. Among the lateral load resisting systems, the outrigger and belt truss system has been used most frequently in construction of high-rise buildings with 60 floors or more [1,2]. As shown in Fig. 1, the belt truss is used to tie external reinforced concrete (RC) columns of a high-rise building up with a steel belt truss that are installed over one or two stories. However, the concrete around the embedded steel plate in Fig. 2 can be damaged by the heat input from a long-time (up to 48 hours) onsite welding of the embedded and gusset plates. Especially when the embedded plate is thin and the heat input is large, the embedded steel plate may show so large vertical and horizontal strains that there can be cracks between the embedded plate and concrete and even explosive fracture may occur to high strength concrete with the compressive strength of 50 MPa or higher. However, no clear design standard has been established for the evaluation or experimental tests for the excessive deformation or damage caused by the welding heat from the plates.

Various thermal modelling or experimental tests have been conducted to simulate welding deformation of steel plates [3-9]. The thermos-elastic-plastic finite element analysis was also applied to temperature variation of steel plate, and a formula for calculation of temperature distribution was proposed [10,11]. Experimental data obtained by the other studies were utilized to prove the accuracy of the formula [12]. Another attempt was to replace 3D modeling by 2D modeling for effectively analyzing results in shorter time, and an optimal method was found, which produced the same results but saved 40% time [13,14]. The expansion of concrete using fly ash and blast-furnace slag at different temperatures (10, 20 and 30 ?) was evaluated in terms of the materials. It turned out that the two parameters of fly ash and blast-furnace slag changed the contraction of high strength concrete containing them [15-17].

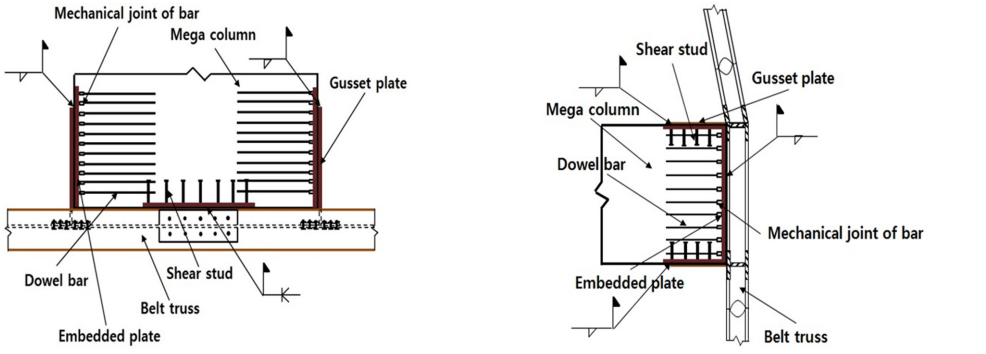
The increase in the thickness of thin steel plate constrained concrete very effectively, thereby improving the structural performance, and the concrete columns reinforced with thin square steel plate showed higher axial capacity than those reinforced with thin circular or elliptical steel plate [18]. The stirrups using high strength wire of concrete columns were analyzed. It turned out that such high strength stirrups produced more effective

†Corresponding author: Park, Hyo Seon
E-mail: hspark@yonsei.ac.kr




(a) Floor plan (b) RC mega columns and a steel belt truss

**Figure 1.** Floor plan and belt truss in a high-rise building with the outrigger and belt truss system.




**(a) A partial welding of the mega column and belt truss joint**

**(b) Full welding of the 3 sides of the mega column and belt truss joint**

**Figure 2.** Gusset and embedded plates for a joint between RC mega column and steel belt truss.

constraint of concrete columns than the conventional stirrups, thereby being effective for axial loads and ductility [19]. In addition, when various warp materials like carbon or aramid were used to surround concrete columns, the axial capacity and ductility were clearly improved [20]. Recently, construction methods for a joint between reinforced concrete shear wall and steel girders have been tested experimentally to analyze the effect of heat input from long-time onsite welding on the slender concrete shear wall [21-23].

The existing studies so far revealed that the analytical evaluation of concrete cracks due to the welding heat has been very difficult in many techniques adopting diverse detailed conditions. Also, a literature review showed insufficient research on evaluation of concrete damage or cracks due to the heat input from a relative long welding of embedded steel plate in RC columns. Accordingly, appropriate experiments are needed for accurate evaluation of the effect of the welding on RC columns. Moreover, the evaluation of crack-related structural stability needs to be performed for each construction method, and an efficient crack reduction method that could be applicable on site is to be developed and validated.

In this study, experimental tests of the joint between RC column and steel belt truss have been conducted with full-scale specimens composed of materials with the same strengths as those of the actual high-rise building structure. To analyze the effect on the heat input on RC column, column specimens with embedded steel plates for the experimentation are classified into four different types. Through full-scale experiments of four RC columns with steel plates with different details, the effects of long-time welding of the embedded and gusset plates on the high strength concrete were analyzed based on three aspects: 1) temperature measurements, 2) pattern and characteristics of cracks, and 3) effect of cracks on the compressive strength of RC column.

## 2. Outline of Experiments

In order to analyze the effect of long-time welding heat on performance of the concrete column in high-rise

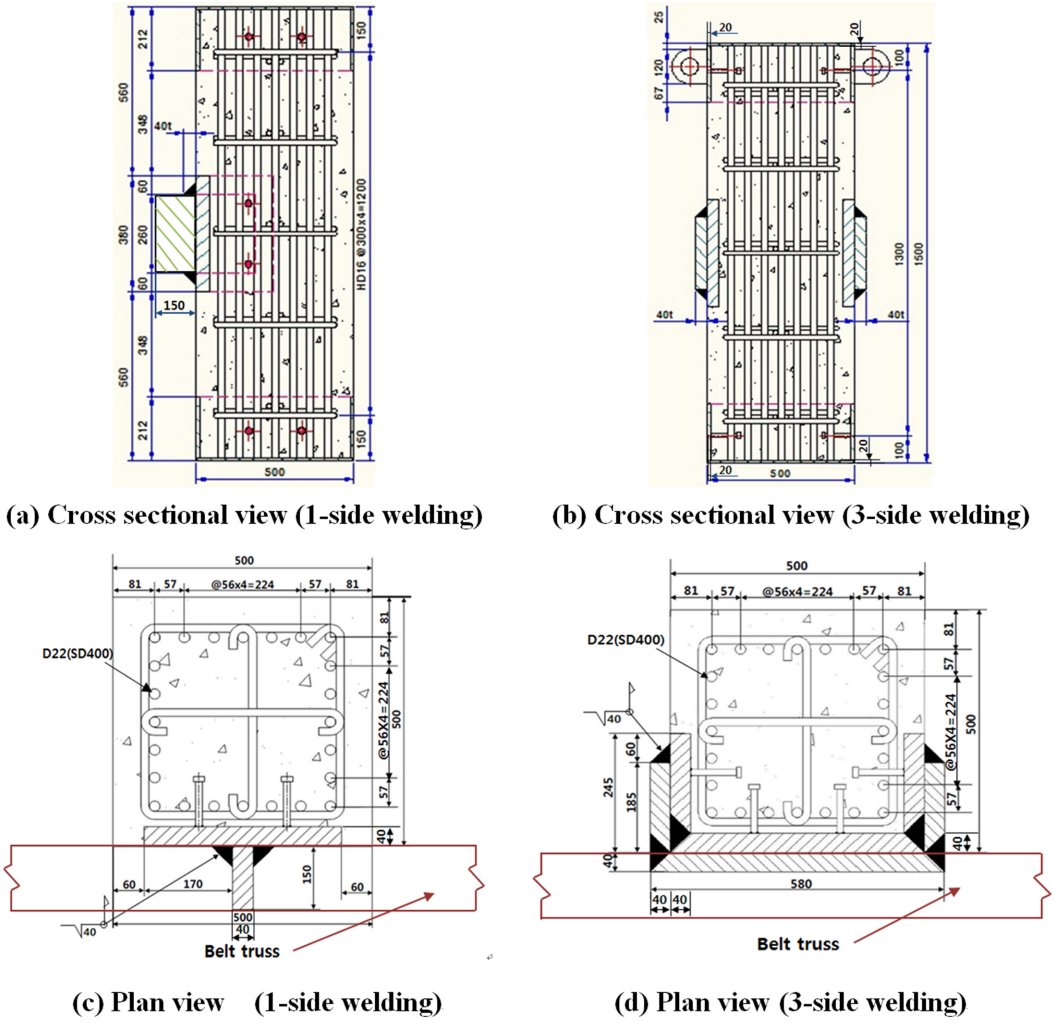



**Figure 3.** Details of the specimen.

buildings at construction sites, two different the compressive strengths of concrete for the specimens were 55 and 80 MPa, which are frequently used in columns of high-rise buildings. As shown in Fig. 3, to make the joint between the belt truss and RC column, the gusset plate has been welded to the embedded steel plate in two different types of welding processes: 1-side welding with single steel plate embedded in one side of the column (Fig. 3(a&c)) and 3-side welding with three steel plates embedded in 3 sides of the column (Fig. 3(b&d)). Then, the experiment was conducted under 4 different conditions: 55 MPa, 80 MPa, 1-side welding, and 3-side welding.

### 2.1 Full-scale Experimental Specimens

Concrete with compressive design strength of 55 MPa and 80 MPa, which were applied in a real high-rise building site, were used for specimens. As shown in Fig. 3, D22 and SD400 (Fy = 400 MPa) were used for rebars for the specimens with the dimension of 500 mm (width) × 500 mm (width) × 1,500 mm (length). The thickness of rebar cover was set to 80 mm. The welding was performed after 28 days of concrete curing. As can be seen in Fig. 3(a) and (b), steel mold and shear studs were installed at both upper and lower part of the column to lift the specimen.

As shown in Fig. 3(a&c), the embedded plate for 1-side welding had the size of 380 mm (width) × 380 mm (length) × 40 mm (thickness). For 3-side welding, as shown in Fig. 3(b&d), the embedded plate had the size of 910 mm (width) × 380 mm (length) × 40 mm (thickness). SM490 (Fy = 325 MPa) was used for the embedded plate. As for the gusset plate attached on the top of the embedded steel plate, the size of 950 mm (width) × 260 mm (length) × 40 mm (thickness) was applied to 3-side welding, while the size of 200 mm (width) × 260 mm (length) × 40 (thickness) was adopted for 1-side welding.

The experimental variables were classified into four types: TS1-55, with the concrete strength of 55 MPa and 1-side welding; TS1-80, with the concrete strength of 80 MPa and 1-side welding; TS3-55, with the concrete strength of 55 MPa and 3-side welding; TS3-80, with the concrete strength of 80 MPa and 3-side welding. Table 1

**Table 1.** Experimental test results of compressive strength of concrete

| Concrete design strength | Curing of concrete (days) | Compressive design strength ($N/mm^2$) | Compressive strength ($N/mm^2$) | Young's modulus (GPa) |
|---|---|---|---|---|
| 55 MPa | 28 | 55 | 56.8 | 34.1 |
| 80 MPa | 28 | 80 | 80.8 | 37.6 |

**Table 2.** Experimental test results of steel members and studs

| Steel grade | Yield strength ($N/mm^2$) | Tensile strength ($N/mm^2$) | Young's modulus (GPa) | Elongation rate (%) |
|---|---|---|---|---|
| SM490 | 428.3 | 518.3 | 207.5 | 24.5 |

and 2 present the test results of mechanical properties of the concrete and steel members used for specimens, respectively.

### 2.2 Experimental Method

For TS1-55 and TS1-80 specimens in Fig. 4(a), the gusset plate is welded to the embedded plate in a total of 20 passes (in the same way in welding process in the field, each side is welded 10 times). For TS3-55 and TS3-80 specimens in Fig. 4(b), the gusset plate is welded to the embedded plate in a total 10 passes (1 pass means 1 welding of one side). The welding in the experiment was performed in the same way as the onsite welding, and the mean voltage, the mean current, and the weld time were measured to be 41V, 312A, and 13-17min/pass, respectively. To analyze the effect or damage on RC column due to the welding heat, cracks and strains of specimens were checked after each pass of welding was finished.

As shown in Fig. 5, the test specimens were fabricated in four steps: (a) fabrication and placement of rebars with strain gauges, (b) fabrication of steel mold and formwork to pour the concrete, (c) removing the formwork and curing the concrete after 28 days, and (d) making of crack locations after each pass of welding.

### 3.1. Temperature Measurement Results

As shown in Fig. 7, a laser gun (infrared digital non-contact laser thermometer that reads a temperature by shooting a laser to a point for 3 seconds) was used to measure temperatures of concrete and embedded steel plate. For all specimens, the temperature at the surface of the concrete was measured at 50 mm from the edge of the embedded plate. Then, the temperatures of the concrete for TS1 and TS3 specimens were measured at 220 mm (Point A in Fig. 7a) and 110 mm (Point C in Fig. 7b) from the edge of the gusset plate, respectively. Temperature at the surface of embedded steel plate was measured at 50 mm from the edge of the gusset plate. As shown in Fig. 7, the points for measurement of temperatures of the gusset plate for TS1 and TS3 specimens were Point B for TS1 and Point D for TS3, respectively. The measurement range of the laser gun was –50°~900°.

For TS1 specimens in Fig. 4a, the joint has been created by a double weld joint where the weld has been welded from both sides (in the same way as in welding process in the field). For TS3 specimens, after completion of 10 passes for the half of the weld length (2,420 mm / 2 = 1,210 mm), a 40 minute break was given before carrying out the remaining half of the weld length since the overall length of the weld of 2,420 mm was relatively long (Fig. 7b).

Table 3 presents temperatures of the embedded plate and the surface of concrete, which were measured during 10 passes of welding on the embedded plates of specimens. Maximum temperatures of the embedded steel plates for TS1-55 and TS1-80 were 306.6°C and 277.1°C, respec-

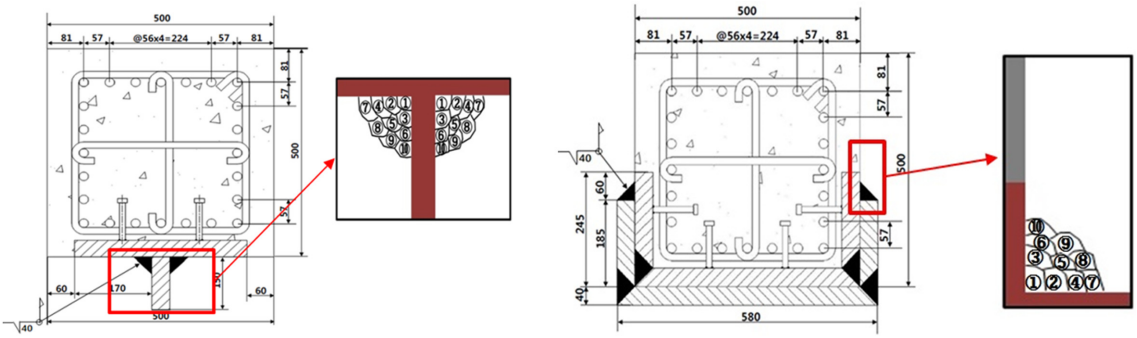



**Figure 4.** Multi-pass fillet welding for the joint.

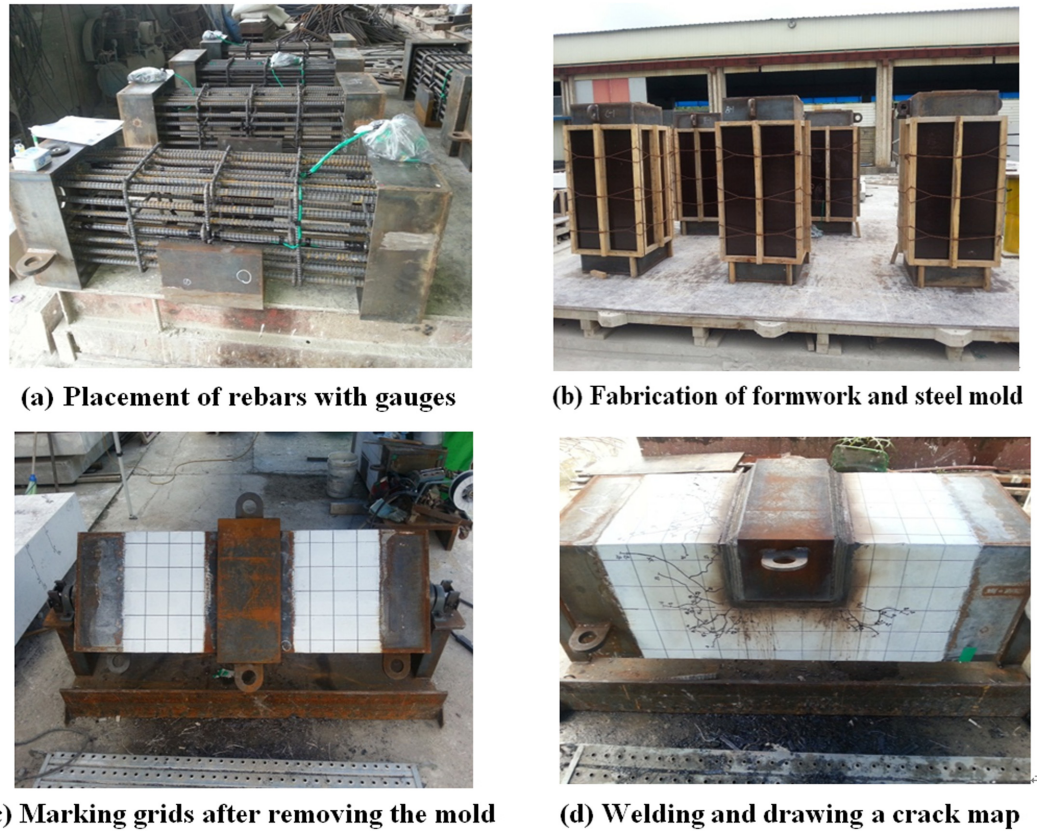


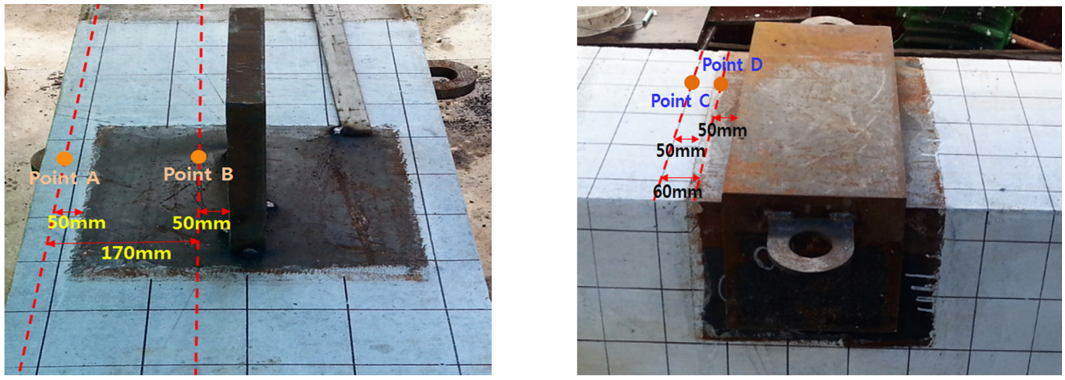

**Figure 5.** Fabrication of specimens.



**Figure 6.** Test setup for application of axial loading using UTM.

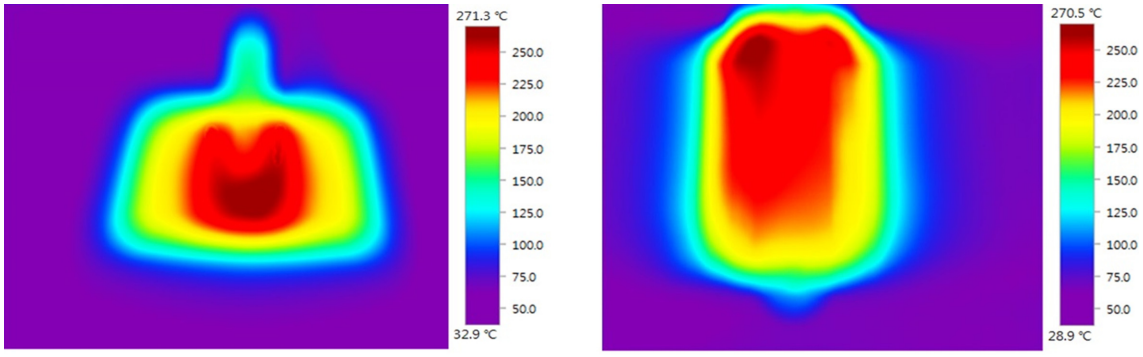
tively. For specimens with the 3-side welding, maximum temperatures of the steel plates for TS3-55 and TS3-80 were 345.3°C and 351.3°C, respectively. In the case of temperature at the surface of concrete, maximum temperatures of concrete for TS1-55 and TS1-80 were 114.1°C and 140.4°C, respectively. For the 3-side welding, maximum temperatures of concrete for TS3-55 and TS3-80 were 140.7°C and 148.6°C, respectively. Since the weld length of 1,210 mm for TS3 specimen is longer than the weld length of 600 mm for TS1 specimen, temperatures measured at both the surface of concrete and steel embedded plate of TS3 specimens were higher than those for TS1 specimens. The maximum temperatures for concrete and steel plates for the specimens are compared at Fig. 9. When TS1-55 and TS3-55 were compared, the embedded plate and the concrete of TS3-55 had higher temperatures by 38.7°C and 26.6°C, respectively. As shown in Fig. 8, when measured with a thermal image detector (GDL700E+) [24], the TS3-55 specimen showed the heat distribution area of high temperatures was relatively small in the concrete part near the embedded plate. Also, when TS1-80 and TS3-80 were compared, the embedded plate and the concrete of TS3-80 had higher temperatures by 74.2°C and 8.2°C respectively.

In addition, among TS3 specimens, TS3-80 had higher temperatures both in the embedded plate and the concrete by 6°C and 7.8°C respectively. Among TS1 specimens, TS1-55 showed 29.5°C higher temperature of the embedded plate but 26.3°C lower temperature of the concrete. In other words, the specimens with the compressive strength of 80 MPa produced a higher temperature of concrete than those with 55 MPa. This may indicate that heat transfer was facilitated by small voids in high strength




(a) TS1 specimen (b) TS3 specimen

**Figure 7.** Temperature checking points using a laser thermometer.




(a) TS1-55 (b) TS3-55

**Figure 8.** Thermal image detector test results for TS1-55 and TS3-55 specimens.

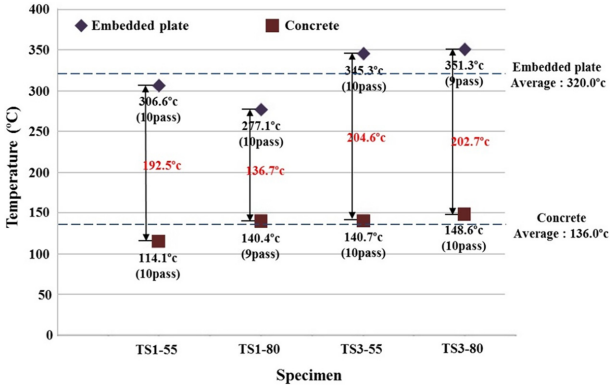



**Figure 9.** Comparison of the maximum temperatures between the embedded plate and the concrete by using a laser gun.

concrete. Scanning electron microscope (SEM) images for concrete with different compressive design strengths used for specimens are shown in Fig. 10.

### 3.2 Crack Patterns due to Welding and Loading

Crack analysis of 4 specimens divided two cases of welding and loading. After completion of the welding, in the case of welding crack marked by black lines in Fig. 11, cracks in the specimen are visually inspected and marked at the surface of the specimen. The visual inspection revealed that 3-side welding caused more cracks on a specimen than 1-side welding, as shown in Fig. 11, and the welding heat generated more micro cracks (less than 0.3 mm width) in 80 MPa concrete than in 55 MPa concrete.

In the case of loading crack marked by red lines in Fig. 12, the maximum crack width (3 mm) of the specimen using 55 MPa concrete was larger than that (1 mm) of the specimen using 80 MPa concrete. Besides, loading did not develop welding cracks nor increase the crack width. Unlike welding cracks in the middle of specimens, loading made cracks concentrated on the top, the bottom and the compressed surface of the specimens. As a result, even if onsite welding generated cracks in a column, they were not so deep and wide as to affect the design strength. The crack pattern and distribution in Fig. 11 and 12 display that loading cracks were concentrated in edges and a short side, while welding cracks developed in a radial form and spread along with the increase in the number of welding passes.

### 3.3 Compressive Strength Test

To analyze the effect of long-time onsite welding on the

**Table 3.** The results of temperature measurement of the four specimens (TS - Test Specimen, measured by a laser gun)

| Pass | TS1-55 (1-side; 55 MPa) | | TS1-80 (1-side; 80 MPa) | | TS3-55 (3-side; 55 MPa) | | TS3-80 (3-side; 80 MPa) | |
|---|---|---|---|---|---|---|---|---|
| | Embed plate | Concrete | Embed plate | Concrete | Embed plate | Concrete | Embed plate | Concrete |
| 1 | 155.5 | 26.8 | 100.2 | 33.4 | 156.2 | 30.3 | 184.2 | 41.7 |
| 2 | 161.4 | 37.7 | 133.4 | 46.2 | 234.4 | 56.2 | 235.5 | 63.6 |
| 3 | 163.3 | 49.0 | 203.1 | 63.5 | 241.1 | 115.5 | 245.4 | 103.5 |
| 4 | 177.4 | 82.9 | 196.3 | 90.8 | 252.5 | 120.3 | 251.4 | 102.4 |
| 5 | 222.8 | 73.1 | 208.2 | 95.3 | 263.3 | 125.4 | 281.3 | 107.3 |
| 6 | 232.6 | 83.8 | 220.5 | 102.4 | 269.4 | 115.2 | 283.3 | 100.2 |
| 7 | 233.6 | 106.6 | 246.6 | 108.3 | 274.3 | 123.8 | 297.6 | 114.3 |
| 8 | 256.3 | 112.6 | 274.2 | 120.2 | 294.1 | 130.1 | 329.9 | 134.3 |
| 9 | 299.9 | 105.3 | 272.3 | 140.4 | 332.2 | 137.2 | 351.3 | 134.4 |
| 10 | 306.6 | 114.1 | 277.1 | 137.3 | 345.3 | 140.7 | 334.7 | 148.6 |

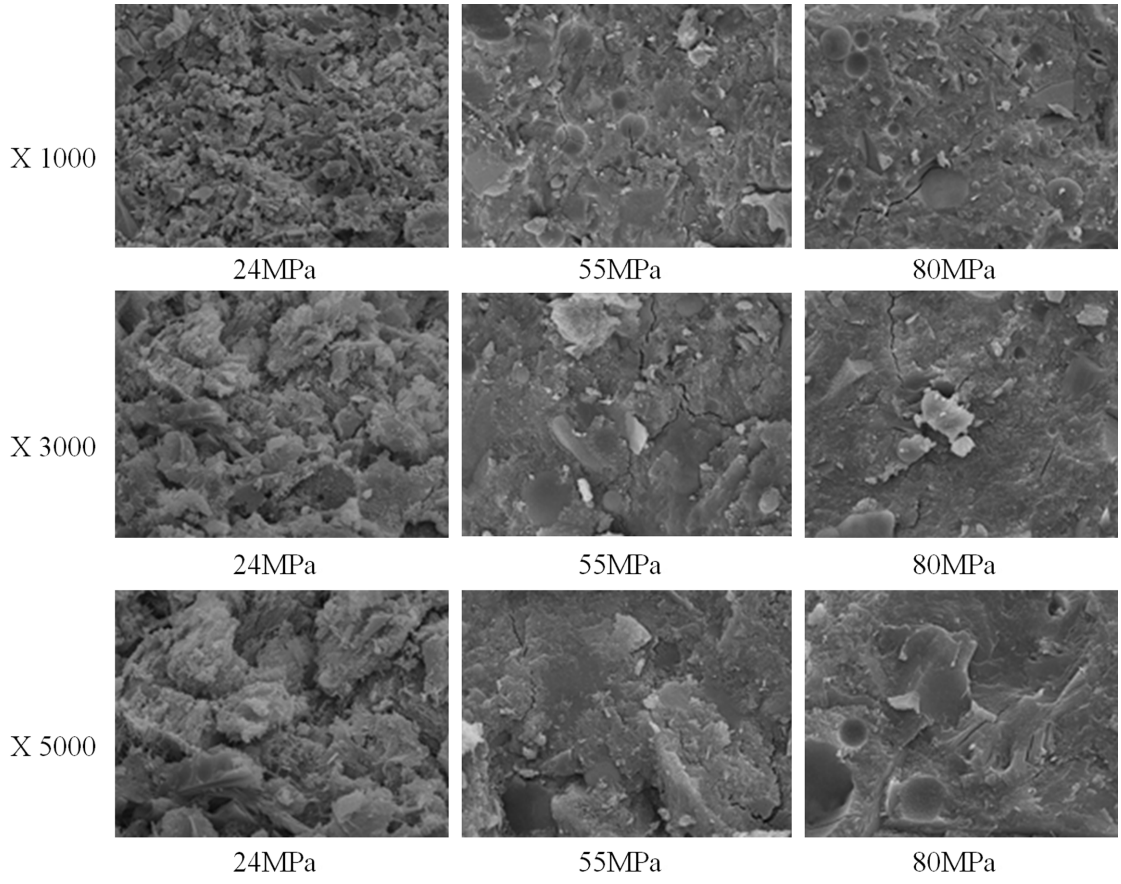



**Figure 10.** SEM images for concrete with different design strengths.

high-strength concrete column for the joint between gusset plates and the embedded plate, the change in the compressive strength of concrete due to the welding cracks was examined by compressive loading test in Fig. 6. The relationships between the load and displacement of the column specimens subjected to 80%, 100%, and 120% of compressive design strengths were measured through monotonic loading of UTM in displacement control rate of 0.002 mm/sec.

As shown in Fig. 13 and Table 4, all of the specimens endured 80%, 100% and 120% of the design strength without degradation of axial load bearing capacity. As shown in Fig. 11, the comparison between TS1-55 and TS3-55 specimens revealed that TS3-55 had a larger displacement under the same load (1.2 mm increase under the design strength). On the other hand, when TS1-80 and TS3-80 specimens were compared, TS3-80 had a smaller displacement under the same load (0.4 mm decrease under

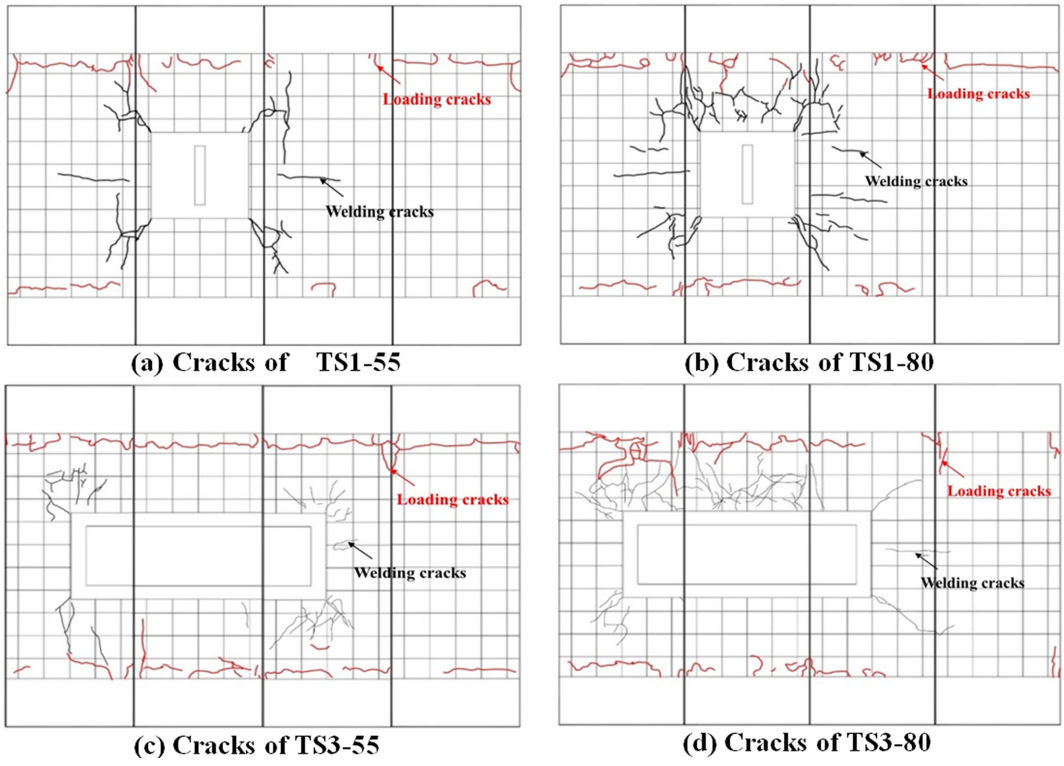



**Figure 11.** Cracks of specimens due to the welding and loading.

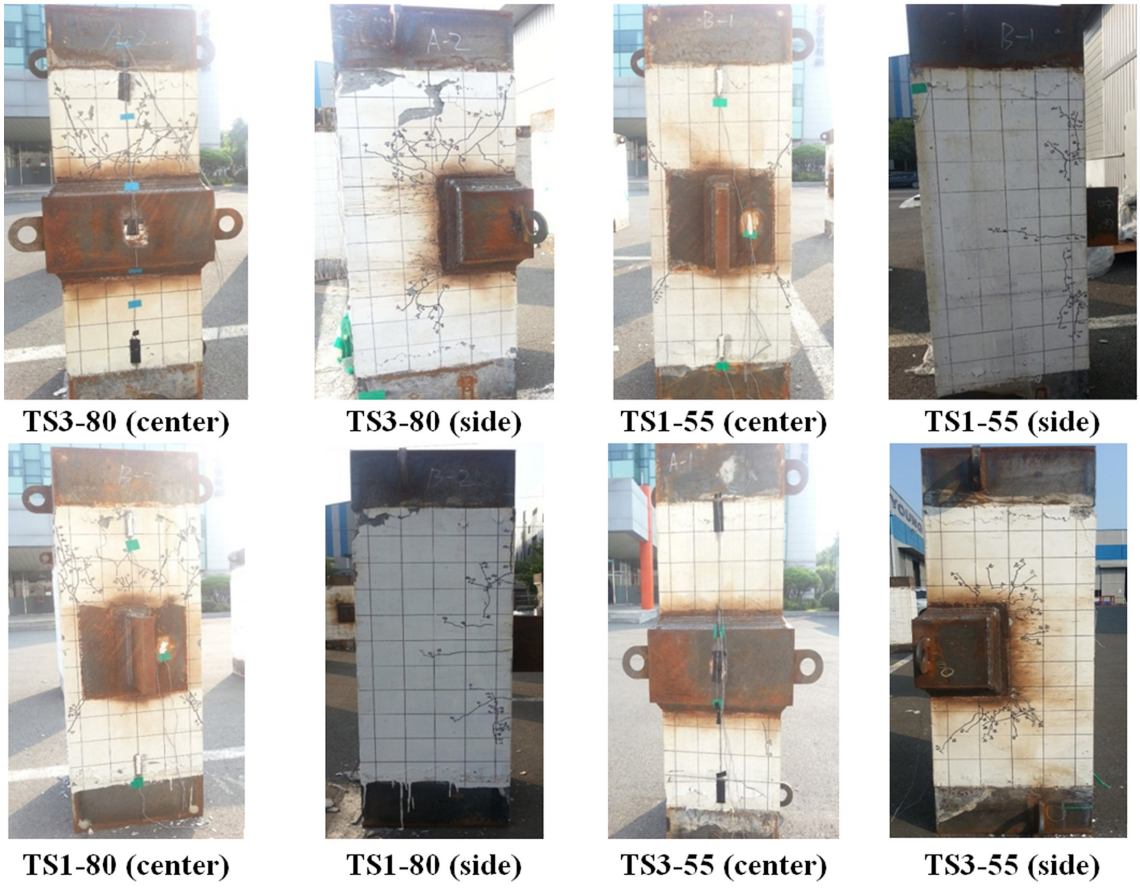



**Figure 12.** Cracks image after the compressive loading test

**Table 4.** Load–displacement responses of specimens subjected to 80%, 100%, 120% of design strengths

| Specimen | Test results | Displacement | Remarks |
|---|---|---|---|
| TS1-55 (1-side; 55 MPa) | 6,381 kN (80% of design strength) | 9.8 mm | No brittle fracture |
| | 7,976 kN (100% of design strength) | 11.2 mm | |
| | 9,571 kN (120% of design strength) | 12.5 mm | |
| TS1-80 (1-side; 80 MPa) | 8,423 kN (80% of design strength) | 11.5 mm | No brittle fracture |
| | 10,529 kN (100% of design strength) | 13.3 mm | |
| | 12,635 kN (120% of design strength) | 14.7 mm | |
| TS3-55 (3-side; 55 MPa) | 6,381 kN (80% of design strength) | 11.2 mm | No brittle fracture |
| | 7,976 kN (100% of design strength) | 12.4 mm | |
| | 9,571 kN (120% of design strength) | 14.0 mm | |
| TS3-80 (3-side; 80 MPa) | 8,423 kN (80% of design strength) | 11.2 mm | No brittle fracture |
| | 10,529 kN (100% of design strength) | 12.9 mm | |
| | 12,635 kN (120% of design strength) | 14.7 mm | |

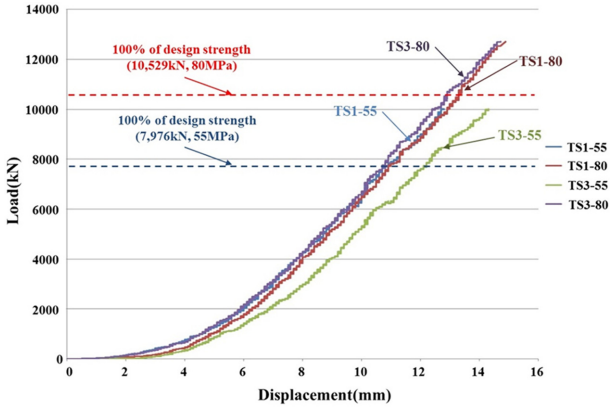



**Figure 13.** Load-displacement graphs for specimens subjected to 80%, 100%, 120% of design strength.

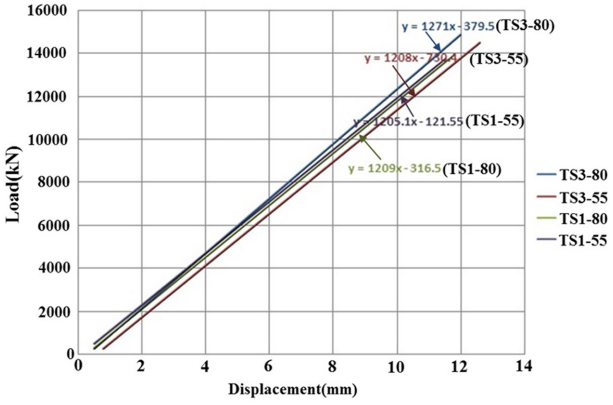



**Figure 14.** Initial stiffness of specimen.

the design strength). Accordingly, even though the long-time onsite welding on the high-strength concrete column for the joint could result in concrete cracks, the axial capacity of the column would not be affected and the increase and decrease of displacements would not show any regular pattern.

Using the load-displacement graphs from the loading test in Fig. 13, the initial stiffnesses of 4 specimens were compared. The largest initial stiffness was 1,271 kN/mm in TS3-80, followed by 1,209 kN/mm in TS1-80, 1,208 kN/mm in TS3-55 and 1,205 kN/mm in TS1-55. As shown in Fig. 14, when the concrete strength was 80 MPa, the initial stiffness was higher than the concrete strength of 55 MPa, and moreover, TS3-80 showed a higher initial stiffness than TS1-80, and TS3-55 had a higher initial stiffness than TS1-55. The experimental results clarified that TS3-80 had the highest initial stiffness but the remaining specimens of TS1-80, TS3-55 and TS1-55 showed only a slight difference, that is, similar initial stiffness. Consequently, it turned out that concrete cracks due to long-time onsite welding have no effect on the degradation of the stiffness of a concrete column.

During the compressive loading test, the strains were measured by installing strain gauges at vertical rebars (top, middle, bottom), outer surface concrete (top, middle, bottom), and the middle of horizontal rebars (lateral ties), as shown in Fig. 15. The load-strain curves obtained from the compression test for TS1-50 are given in Fig. 15. For the reference specimen of TS1-50, when a load is applied, the top of concrete is the first part that endures the stress, followed by the bottom and the middle of concrete. Then, the stress is transmitted to the middle, top and bottom of a vertical rebar, followed by lateral ties. Every specimen displayed a similar pattern of load-strain relationship, as shown in Fig. 15, and especially, the top of concrete had a larger initial strain. For the loads of 3,988 kN and 5,265 kN, which corresponded to the design strength/2, and 7,976 kN and 10,529 kN, which are the design strength, as shown in Fig. 15, when the average strain for the top, middle and bottom of the vertical rebar of each specimen was calculated by using the strain results of vertical rebars

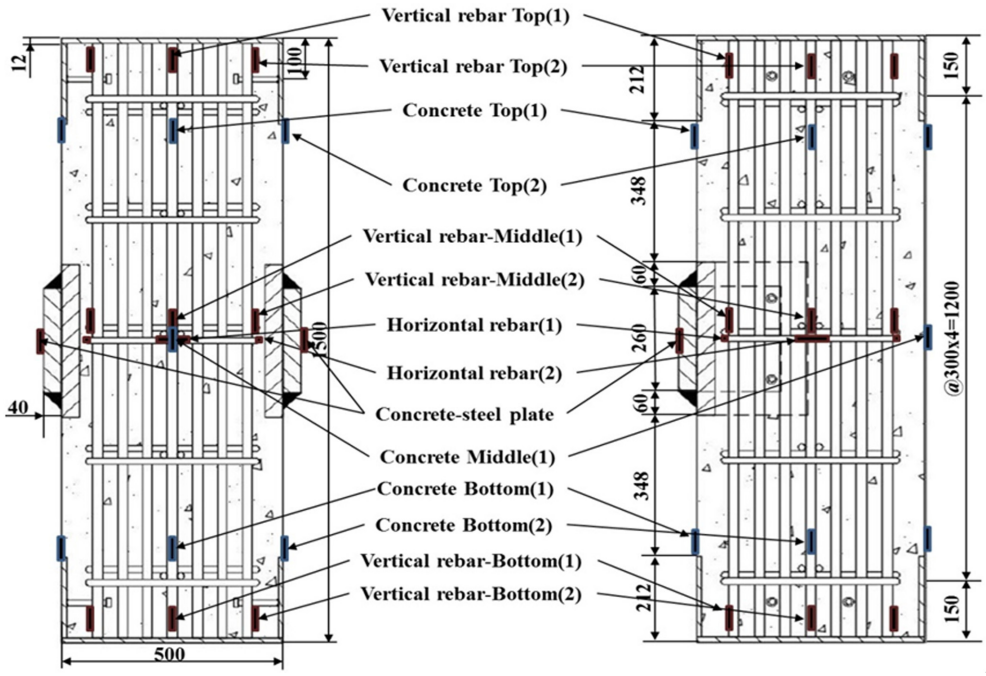



**Figure 15.** Locations of gauges for measurement of strains.

in Table 5, each specimen had the following average strain : TS1-55 (0.00221, 0.00229), TS1-80(0.00050, 0.00212), TS3-55(0.00222, 0.00528) and TS3-80(0.00299, 0.00612). TS1-55 showed a higher strain of vertical rebar than TS3-55, and TS3-80 had a higher strain of vertical rebar than TS1-80. It turned out that the strain of vertical rebar tended to increase along with the increase of welding amount.

Again, for the loads of 3,988 kN and 5,265 kN, which corresponded to the design strength/2, and 7976 kN and 10,529 kN, which are the design strength, when the average strain for the top, middle and bottom of the vertical rebar of each specimen was calculated by using the strain results of concrete in Table 5, each specimen had the following average strain : TS1-55(0.00859, 0.01239), TS1-80(0.00183, 0.00465), TS3-55(0.00590, 0.00775) and TS3-80(0.00734, 0.01047). TS1-55 showed a higher strain of concrete than TS3-55, and TS3-80 had a higher strain of concrete than TS1-80. It turned out that the strain of concrete did not show any regular pattern when the welding amount increased.

For the loads of 3,988 kN and 5,265 kN, which corresponded to the design strength/2, and 7,976 kN and 10,529 kN, which are the design strength, when the strain results of lateral ties in Table 5 were averaged, each specimen showed the following results : TS1-55(0.00066, 0.000093), TS1-80(0.00019, 0.00038), TS3-55(0.00012, 0.0004) and TS3-80(0.00018, 0.00038). In addition, when the strain results of the embedded steel plate were averaged, TS1-55 had 0.00013 and 0.000007, TS1-80 had 0.00007 and 0.00012, TS3-55 showed 0.00005 and 0.00005, and TS3-80 showed 0.00010 and 0.00016. Consequently, 4 specimens did not display any significant difference of strain both in the lateral tie and the embedded steel plate, and the increase and decrease of strain were very small.

**Table 5.** Comparison of strain results at vertical rebars, lateral ties, and concrete of 4 specimens

| Locations for strain gauges | Strain (με) | | | | | | | |
|---|---|---|---|---|---|---|---|---|
| | Design strength/2 | | | | Design strength | | | |
| | TS1-55 | TS1-80 | TS3-55 | TS3-80 | TS1-55 | TS1-80 | TS3-55 | TS3-80 |
| Vertical rebar top | 0.00257 | 0.00029 | 0.00242 | 0.00355 | 0.00562 | 0.00162 | 0.00701 | 0.00777 |
| Vertical rebar middle | 0.00258 | 0.00062 | 0.00269 | 0.00391 | 0.00507 | 0.00236 | 0.00519 | 0.00680 |
| Vertical rebar bottom | 0.00149 | 0.00058 | 0.00156 | 0.00152 | 0.00319 | 0.00237 | 0.00363 | 0.00378 |
| Lateral tie(1) | 0.00065 | 0.00008 | 0.00011 | 0.00017 | 0.00075 | 0.00010 | 0.00039 | 0.00050 |
| Lateral tie(2) | 0.00067 | 0.00029 | 0.00013 | 0.00018 | 0.00111 | 0.00065 | 0.00041 | 0.00025 |
| Concrete top | 0.02062 | 0.00456 | 0.01366 | 0.01290 | 0.02575 | 0.00927 | 0.01552 | 0.01290 |
| Concrete middle | 0.00256 | 0.00031 | 0.00269 | 0.00695 | 0.00505 | 0.00233 | 0.00547 | 0.00380 |
| Concrete bottom | 0.00258 | 0.00062 | 0.00136 | 0.00216 | 0.00636 | 0.00235 | 0.00226 | 0.01470 |
| Embedded steel plate | 0.00013 | 0.00007 | 0.00005 | 0.00010 | 0.00007 | 0.00012 | 0.00005 | 0.00016 |

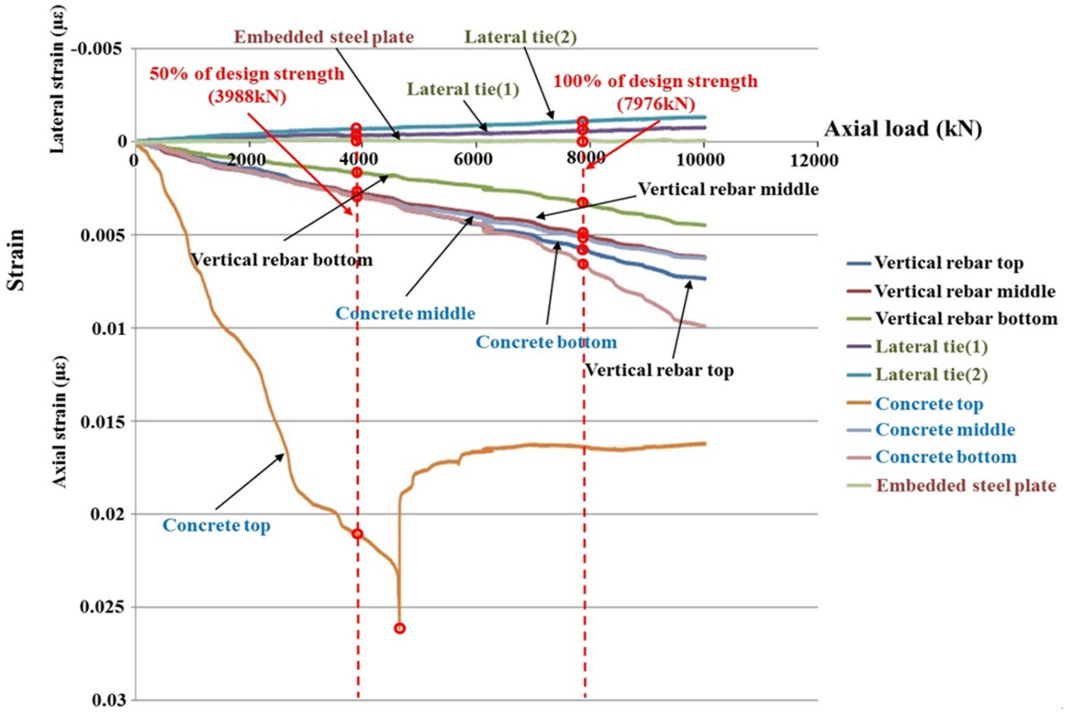



**Figure 16.** Strains measured from gauges attached at vertical rebars, lateral ties, and concrete of TS1-55.

## 4. Conclusions

To investigate the effect of a long time welding on concrete around embedded steel plate for a joint between RC column and steel belt truss, four different types of specimens were tested and analyzed in terms of three items: 1) temperature distribution measurements, 2) crack patterns due to the welding, and 3) compressive strength tests. The dimensions for the high strength concrete column with two different compressive strengths of 55 and 80 MPa were 500 mm (width) × 500 mm (width) × 1,500 mm (length). The gusset plates made of SM490 (Fy = 325 MPa) were welded over the embedded plates after 28 days of curing of concrete of the column. The dimensions for the gusset plates for TS1 and TS3 specimens are 200 mm (width) × 260 mm (length) × 40 (thickness) and 950 mm (width) × 260 mm (length) × 40 mm (thickness), respectively.

From the results of the temperature measurements of four specimens, maximum temperatures measured at the surface of concrete for TS1 and TS3 specimens were 140.4°C and 148.6°C, respectively. For specimens with the same weld length, specimens with the compressive strength of 80 MPa produced a higher temperature of concrete than those with 55 MPa since heat transfer was facilitated by small voids in high strength concrete. Due to the heat input from the welding, welding cracks developed in a radial form and spread along with the increase in the number of welding passes. The visual inspection revealed that 3-side welding caused more cracks on a specimen than 1-side welding, and the welding heat generated more micro cracks in 80 MPa concrete than in 55 MPa concrete.

To analyze the effect of cracks due to the long-time onsite welding on the high-strength concrete column, the change in the compressive strength of concrete was examined by compressive loading test. Based on the compressive tests, it is found that the axial capacity of the column was not affected even though the heat input up to about 150°C from the long-time onsite welding on the high-strength concrete column for the joint could result in concrete cracks. For the case of the initial stiffness based on the load-displacement graphs, it is also turned out that concrete cracks due to the heat input of about 150? from the long-time onsite welding have no effect on the degradation of the stiffness of a concrete column.

## Acknowledgements

This research was supported by a grant (Code# '09 R&D A01) from the Cutting-edge Urban Development Program funded by the Ministry of Land, Transport and Maritime Affairs of the Korean government

This work was supported by the National Research Foundation of Korea (NRF) grant funded by the Korea government (MSIP) (NRF-2018RIA5A1025137)

## References

Taranath, B.S. (2010). "Reinforced concrete design of tall buildings." CRC Press. Boca Raton. FL.

Park, H.S., Lee, E., Choi, S.W., Oh, B.K., Cho, T., Kim, Y.

(2016). "Genetic-algorithm-based minimum weight design of an outrigger system for high-rise buildings." *Eng. Struct*., 117(5), 496-505.

Zong, L., Shi, G., Wang, Y. (2015). "Experimental investigation and numerical simulation on fatigue crack behavior of bridge steel WNQ570 base metal and butt weld." *Constr. Build. Mater*., 77(15), 419-429.

Pan, J., Chen, S., Lai, Z., Wang, Z., Wang, J., Xie, H. (2017). "Analysis and fracture behavior of welded box beam-to-column connections considering residual stresses." *Constr. Build. Mater*., 154(15), 557-566.

Mollicone, P., Camilleri, D., Gray, T.G.F., Comlekci, T. (2006). "Simple thermo-elastic-plastic models for welding distortion simulation." *J. Mater. Process. Technol*., 176(1-3), 77-86.

Deng, D., Murakawa, H. (2008). "Prediction of welding distortion and residual stress in a thin plate butt-welded joint." *Comput. Mater. Sci*., 43(2), 353-365.

Long, H., Gery, D., Carlier, A., Maropoulos, P.G. (2009). "Prediction of welding distortion in butt joint of thin plates." *Mater. Des*., 30(10), 4126-4135.

Manurung, Y.H.P., Lidam, R.N., Rahim, M.R., Zakaria, M.Y., Redza, M.R., Sulaiman, M.S., Tham, G., Abas, S.K. (2013). "Welding distortion analysis of multipass joint combination with different sequences using 3D FEM and experiment." *Int. J. Press. Ves. Pip*., 111-112, 89-98.

Li, Y., Wang, K., Jin, Y., Xu, M., Lu, H. (2015). "Prediction of welding deformation in stiffened structure by introducing thermo-mechanical interface element" *J. Mater. Process. Technol.*, 216, 440-446.

Pham, T., Kim, S. (2017). "Characteristics of microstructural phases relevant to the mechanical properties in structural steel weld zone studied by using indentation." *Constr. Build. Mater*., 155(30), 176-186.

Mackwood, A.P., Crafer, R.C. (2005). "Thermal modelling of laser welding and related processes: a literature review." *Opt. Laser Technol.*, 37(2), 99-115.

Winczek, J. (2011). "New approach to modeling of temperature field in surfaced steel element." *Int. J. Heat Mass Transf*., 54(21-22), 4702-4709.

Shen, J., Chen, Z. (2014). "Welding simulation of fillet-welded joint using shell elements with section integration, *J. Mater. Process. Technol*." 214(11), 2529-2536.

Alves do Carmo, D., Rocha de Faria, A. (2015). "A 2D finite element with through the thickness parabolic temperature distribution for heat transfer simulations including welding." *Finite Elem. Anal. Des*., 93, 85-95.

Jiang, C., Yang, Y., Wang, Y., Zhou, Y., Ma, C. (2014). "Autogenous shrinkage of high performance concrete containing mineral admixtures under different curing temperatures." *Constr. Build. Mater.*, 61, 260-269.

Hajjar, J.F., Schiller, P.H., Molodan, A., (1998). "A distributed plasticity model for concrete-filled steel tube beam-columns with interlayer slip." *Eng. Struct.*, 20(8), 663-676.

Aly, T., Elchalakani, M., Thayalan, P., Patnaikuni, I. (2010). "Incremental collapse threshold for pushout resistance of circular concrete filled steel tubular columns." *J. Constr. Steel Res*., 66(1), 11-18.

Jamaluddin, N., Lam, D., Dai, X.H., Ye, J. (2013). "An experimental study on elliptical concrete filled columns under axial compression." *J. Constr. Steel Res*., 87, 6-16.

Wei, Y. Wu, Y.F. (2014). "Compression behavior of concrete columns confined by high strength steel wire." *Constr. Build. Mater*., 54, 443-453.

Tiberti, G., Minelli, F., Plizzari, G. (2015). "Cracking behavior in reinforced concrete members with steel fibers: A comprehensive experimental study." *Cem. Concr. Res*., 68, 24-34.

Shim, H.B., Park, H.S. (2017). "Experimental tests on construction methods for a joint between concrete wall and steel girder involving long-time onsite welding." *Constr. Build. Mater.*, 154(8), 600-608.

Li, G., Sun, F., Pang, M. Liu, W. Wang, H. (2016). "Structural Shear Wall Systems with Metal Energy Dissipation Mechanism." *International Journal of High-Rise Building*, 5(3), 195~203.

Park, H.G., Kim, H.J., Park, J.Y. (2019) "Corner steel plate-reinforced core wall system." *International Journal of High-Rise Building*, 8(3), 193~199.

GDL700E+ Industrial thermal image detector. http://hy4989.co.kr/mall/m_mall detail. php?ps_goid=8001.